ACCOUNTS of chemical research

Article

pubs.acs.org/accounts

Ab Initio Molecular Crystal Structures, Spectra, and Phase Diagrams

So Hirata,* Kandis Gilliard, Xiao He,† Jinjin Li, and Olaseni Sode‡

Department of Chemistry, University of Illinois at Urbana−Champaign, 600 South Mathews Avenue, Urbana, Illinois 61801, United States

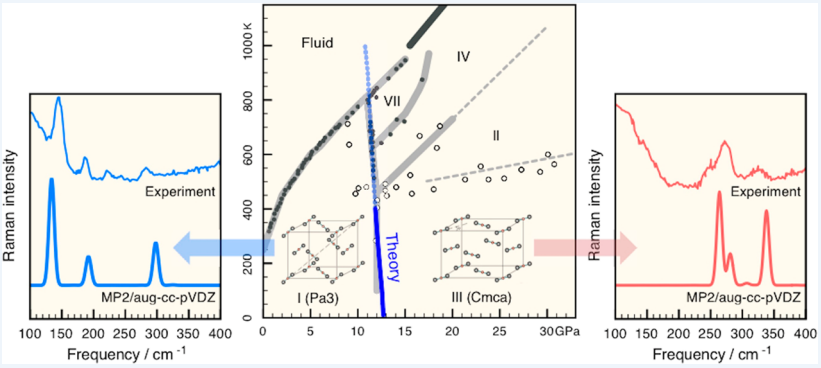

CONSPECTUS: Molecular crystals are chemists' solids in the sense that their structures and properties can be understood in terms of those of the constituent molecules merely perturbed by a crystalline environment. They form a large and important class of solids including ices of atmospheric species, drugs, explosives, and even some organic optoelectronic materials and supramolecular assemblies. Recently, surprisingly simple yet extremely efficient, versatile, easily implemented, and systematically accurate electronic structure methods for molecular crystals have been developed. The methods, collectively referred to as the embedded-fragment scheme, divide a crystal into monomers and overlapping dimers and apply modern molecular electronic structure methods and software to these fragments of the crystal that are embedded in a self-consistently determined crystalline electrostatic field. They enable facile applications of accurate but otherwise prohibitively expensive ab initio molecular orbital theories such as Møller−Plesset perturbation and coupled-cluster theories to a broad range of properties of solids such as internal energies, enthalpies, structures, equation of state, phonon dispersion curves and density of states, infrared and Raman spectra (including band intensities and sometimes anharmonic effects), inelastic neutron scattering spectra, heat capacities, Gibbs energies, and phase diagrams, while accounting for many-body electrostatic (namely, induction or polarization) effects as well as two-body exchange and dispersion interactions from first principles. They can fundamentally alter the role of computing in the studies of molecular crystals in the same way ab initio molecular orbital theories have transformed research practices in gas-phase physical chemistry and synthetic chemistry in the last half century.

In this Account, after a brief summary of formalisms and algorithms, we discuss applications of these methods performed in our group as compelling illustrations of their unprecedented power in addressing some of the outstanding problems of solid-state chemistry, high-pressure chemistry, or geochemistry. They are the structure and spectra of ice I_h, in particular, the origin of two peaks in the hydrogen-bond-stretching region of its inelastic neutron scattering spectra, a solid−solid phase transition from CO_2-I to elusive, metastable CO_2-III, pressure tuning of Fermi resonance in solid CO_2, and the structure and spectra of solid formic acid, all at the level of second-order Møller−Plesset perturbation theory or higher.

INTRODUCTION

Molecular crystals are a large class of solids that consist of well-defined molecular units bound together by weak interactions such as hydrogen-bond, electrostatic (but not ionic), and dispersion interactions. They are ubiquitous since atmospheric species of the Earth and other planets tend to become molecular crystals under pressure.[1,2] Ice (phase I_h of solid H_2O),[3−5] dry ice (phase I of solid CO_2),[6] and solid hydrogen[7] are just three such examples. In addition to the geochemical and planetary science relevance, they are becoming more important with the increasing ability of synthetic chemists to fashion molecules that aggregate into superstructure,[8−10] which, if crystalline, can be molecular crystals. Some explosives are molecular crystals;[11] most drugs are molecular crystals;[12] they are also starting materials of solid-state chemical reactions.[8]

Molecular crystals are chemists' solids, so to speak, because some aspects of their properties can be understood in terms of those of their constituent molecules merely perturbed by a crystalline environment. This is owing to the weakness of intermolecular interactions, which, however, also creates difficulty because it brings about structural complexity known

Special Issue: Beyond QM/MM: Fragment Quantum Mechanical Methods

Received: January 30, 2014
Published: April 22, 2014

   dx.doi.org/10.1021/ar500041m | Acc. Chem. Res. 2014, 47, 2721−2730

as *polymorphism*.[13] It means that there are at least two stable arrangements of molecules in the solid state. This is a rule rather than an exception. As McCrone put it,[14] "the number of forms known for a given compound is proportional to the time and money spent in research on that compound." The truth of this statement made in 1965 is apparent in the aforementioned examples: the number of molecular phases for ice (solid H_2O) is currently 8 (out of 15 crystalline phases) and counting;[5] the numbers for solid CO_2 and H_2 have also been rising steadily with time.[6,7]

Characterization of polymorphs by experimental means alone is difficult for a number of reasons. Most of these polymorphic phases occur at high pressures and low temperatures. Their samples are, therefore, hard to prepare, store, and share. The free energy differences between two phases can be on the order of a few kilojoules per mole or less, in which entropic contributions can be substantial, often causing large hysteresis in phase transitions and obscuring phase boundaries. Coexistence and metastability of phases are also common. The structural changes are often so subtle that an equation-of-state measurement alone is insufficient to draw definitive conclusions; an array of experimental tools, especially diffraction and vibrational spectroscopies, must also be used to reach a reliable conclusion. Equally important is the assistance from accurate computational interpretation and prediction, which is the subject of this Account.

Until very recently, electronic structure calculations for solids meant those based on density-functional theory (DFT) and nearly nothing else. Ab initio molecular orbital (MO) calculations for solids that include electron correlation effects were unthinkable, barring some exceptions,[15−19] because of their prohibitively high computational cost, which increases as at least the fifth power of size. There are, however, two reasons why DFT is less than ideal for our purpose,[20] and we need to resort to ab initio MO theory despite its cost. First, most contemporary exchange-correlation functionals of DFT do not describe dispersion, an essential cohesive force in molecular crystals, although corrections for this deficiency have been proposed.[21] Second, approximations in DFT are nonsystematic in the sense that their errors cannot be controlled, and thus it presently falls short of being a predictive theory.[22] Since the strengths of chemical interactions (intramolecular covalent to intermolecular dispersion) in molecular crystals span 3 orders of magnitude (100 to 0.1 kJ mol^{-1}), we need a predictive theory.

This Account reviews a surprisingly simple yet systematically accurate and efficient scheme of applying ab initio electron-correlated MO theories such as Møller−Plesset perturbation (MP) and coupled-cluster (CC) theories[23] to molecular crystals. We call the scheme an *embedded-fragment scheme*[24−33] because it divides an infinitely extended molecular crystal into monomers, overlapping dimers, etc., which are embedded in the crystal's electrostatic environment. These embedded fragments are, in turn, described by accurate *molecular* electron-correlated theories. In this way, a whole arsenal of molecular methods developed and refined in the past half century for a variety of molecular properties can be applied to solids with a minimum of development efforts.

We are neither the only nor the first group to use the concept of embedded fragmentation. In fact, a large and increasing number of groups today use similar ideas to study biological macromolecules, molecular clusters, crystals, and liquids, which attests to this idea's unparalleled merit. A comprehensive review on this class of methods was written by Gordon et al.,[34] and a Special Issue[35] of *Physical Chemistry Chemical Physics* was organized on the same topic. See also other literature.[36−39] We are, however, among a smaller group[16,40−48] that has applied them systematically to molecular crystals, studying their structures, spectra, and phase diagrams. In this Account, therefore, we focus on our applications of this general scheme to molecular crystals and illustrate its unprecedented power in addressing outstanding questions of solids raised by experimentalists. We keep the discussion of our algorithmic details and taxonomy to a minimum. Instead, through these example applications, we hope to convey the sense that this scheme is likely to extend its reach rapidly to a much wider class of chemical systems and properties and may indeed prove to be one of the most fruitful ideas of computational chemistry in this decade.

COMPUTATIONAL APPROACH

The electronic enthalpy per unit cell, H_e, of a three-dimensional, infinitely extended, periodic molecular crystal is approximated accurately by[26,29]

$$H_e = \sum_i E_{i(0)} + \frac{1}{2}\sum_{\mathbf{n}}\sum_{i,j}\{E_{i(0)j(\mathbf{n})} - E_{i(0)} - E_{j(\mathbf{n})}\} + E_{LR} + PV \quad (1)$$

where $E_{i(0)}$ is the energy of the ith monomer in the central (0th) unit cell, $E_{i(0)j(\mathbf{n})}$ is the energy of the dimer consisting of the ith monomer in the central unit cell and the jth monomer in the $\mathbf{n}$th unit cell ($\mathbf{n}$ stands for three integers specifying a unit cell), E_{LR} is the long-range electrostatic energy correction (i.e., the long-range part of the Madelung constant), P is the pressure, and V is the unit cell volume. It should be understood that $i = j$ and $\mathbf{n} = 0$ is excluded from the second summation. While the truncation of the many-body expansion after the two-body (dimer) term strikes excellent cost−accuracy balance, one can also truncate the series after the three-body or higher-order term.[24]

The energies of the monomers and dimers are evaluated by *any* electronic structure method implemented in molecular software. It is important to embed the monomers and dimers in an electrostatic field of the crystal. The embedding field is represented by atomic point charges[25] or molecular dipole moments,[24] which are determined self-consistently (at the HF level in our implementation). The self-consistency accounts for the polarization or electrostatic induction effect. Furthermore, basis-set superposition errors (BSSE) can also be eliminated by the Boys−Bernardi function counterpoise correction applied to each dimer.[25] This scheme was inspired by the pair-interaction method of Kitaura et al.,[49] but ours is much simpler than their original method, and all of the individual calculations in our scheme can be carried out with unmodified molecular software.

The first and second derivatives of the enthalpy with respect to atomic coordinates are related to atomic forces and force constants, respectively. The derivatives with respect to lattice constants give lattice forces and Young's modulus. These are obtained efficiently by evaluating[26]

$$\frac{\partial H_e}{\partial x} = \sum_i \frac{\partial E_{i(0)}}{\partial x} + \frac{1}{2}\sum_{\mathbf{n}}\sum_{i,j}\left\{\frac{\partial E_{i(0)j(\mathbf{n})}}{\partial x} - \frac{\partial E_{i(0)}}{\partial x} - \frac{\partial E_{j(\mathbf{n})}}{\partial x}\right\} + \frac{\partial E_{LR}}{\partial x} \quad (2)$$

$$\frac{\partial H_e}{\partial a} = \frac{1}{2}\sum_{\mathbf{n}}\sum_{i,j}\left\{\frac{\partial E_{i(0)j(\mathbf{n})}}{\partial a} - \frac{\partial E_{j(\mathbf{n})}}{\partial a}\right\} + \frac{\partial E_{LR}}{\partial a} + P\frac{\partial V}{\partial a} \quad (3)$$

$$\frac{\partial^2 H_e}{\partial x \partial y} = \sum_i \frac{\partial^2 E_{i(0)}}{\partial x \partial y} + \frac{1}{2}\sum_{\mathbf{n}}\sum_{i,j}\left\{\frac{\partial^2 E_{i(0)j(\mathbf{n})}}{\partial x \partial y} - \frac{\partial^2 E_{i(0)}}{\partial x \partial y} - \frac{\partial^2 E_{j(\mathbf{n})}}{\partial x \partial y}\right\} + \frac{\partial^2 E_{LR}}{\partial x \partial y} \quad (4)$$

etc., again using only molecular quantities supplied by molecular software. Here, x and y can be collective, in-phase coordinates (useful for equilibrium geometry determination) or individual atomic coordinates (necessary for obtaining phonon dispersion and density of states or DOS), while a is a lattice constant. Note that these equations neglect the derivatives of the embedding field strength and are slightly approximate. The geometrical derivatives of dipole moments and polarizabilities can also be computed similarly, furnishing information about infrared (IR) and Raman intensities.[30] As such, the embedded-fragment scheme bypasses the difficult issue of the definitions of dipole moments and polarizabilities in solids.[50,51]

With the phonon dispersion in the entire reciprocal space, we can quantify the effect of temperature T by evaluating its Gibbs energy,[32]

$$G = H_e + U_v - TS_v \quad (5)$$

where U_v and S_v are vibrational internal energy (zero-point energy at $T = 0$) and entropy, respectively. They are, in turn, related to the partition function Z_v by

$$U_v = \frac{T}{\beta K}\frac{\partial \ln Z_v}{\partial T} \quad (6)$$

$$S_v = \frac{1}{\beta K}\frac{\partial \ln Z_v}{\partial T} + \frac{1}{\beta T K}\ln Z_v \quad (7)$$

where $\beta = (k_B T)^{-1}$ and K is the number of wave vectors in the reciprocal unit cell. In the harmonic approximation, the partition function is simply

$$Z_v = \prod_n \prod_{\mathbf{k}} \frac{\exp(-\beta\omega_{n\mathbf{k}}/2)}{1 - \exp(-\beta\omega_{n\mathbf{k}})} \quad (8)$$

where $\omega_{n\mathbf{k}}$ is the frequency of the phonon in branch n and wave vector $\mathbf{k}$. It also gives us constant-volume heat capacity, C_V.

The following is a list of the merits and demerits of this method:

Systematic

The many-body expansion of eq 1 embodies a systematic series of approximations characterized by its truncation rank. The series is convergent at the exact calculation for the whole system using a given electronic structure method. If the electronic structure method is also systematic (such as MP and CC), the whole method becomes predictive because errors can be controlled in principle and even in practice.[46]

Versatile

Any electronic structure method can be used for monomer and dimer calculations, be it HF, MP, CC, excited-state,[24] or even non-size-consistent method. It can compute internal energies, enthalpies, structures, vibrational and electronic spectra (including intensities), heat capacities, Gibbs energies, phase diagrams, etc. The scheme does not rely strongly on the periodic boundary conditions (in the sense that plane waves or Bloch orbitals are never used for electrons) and, therefore, can treat lattice distortions that lift periodic symmetry such as phonon dispersions in the entire reciprocal space and phonon DOS. It is also applicable to nonperiodic solids (such as ice I_h discussed below) and defects and disorders.

Accurate

At the dimer truncation, the scheme includes one- and two-body kinetic, Coulomb (classical electrostatic), exchange (including atom−atom repulsion), and correlation (including dispersion) interactions nearly exactly at a chosen electronic structure level as well as three-body and all higher-order Coulomb interactions at the HF level. The effect of mutual polarization or induction including the hydrogen-bond cooperativity is taken into account. BSSE, which can be substantial for molecular crystals bound by dispersion forces, can also be eliminated easily, which is, however, exceedingly difficult to achieve in ab initio crystal orbital calculations.

Efficient

When applied to a molecular cluster, the cost of this scheme increases linearly with cluster size by simply discarding long dimers (dimers consisting of well-separated monomers). Even for the smallest cluster, the cost increases quadratically with size. If one can afford a full configuration interaction (FCI) calculation for a dimer, for instance, one should be able to run FCI for the corresponding crystal. Parallel second-order Møller−Plesset perturbation (MP2) and coupled-cluster singles and doubles (CCSD) calculations for 3D molecular crystals are routine in our laboratory on a small computer cluster.

Limitations

Currently, our scheme is limited to molecular clusters and crystals and cannot be applied to ionic crystals, covalent crystals, metals, or superconductors, although others have shown that even these can be subject to fragmentation.[16,41,47,52,53] Energy bands cannot be obtained, either, though we have reasons to believe that this limitation can also be overcome soon.[54]

■ ILLUSTRATIVE APPLICATIONS

Ice I_h

Among the at least 15 crystalline phases of (water) ice, hexagonal, proton-disordered ice I_h is the most abundant on the Earth's surface and arguably the most important crystal in nature. In 1993, Li and Ross[55] reported a high-quality spectrum of inelastic neutron scattering (INS) from ice I_h, which showed two distinct peaks in the hydrogen-bond-stretching region (Figure 1), specifically, at 229 and 306 cm^{-1}. They interpreted the two peaks as indication of the existence of "two types of hydrogen bonds" that differed in strength by a factor of 2 (to account for the 1.3 ratio of the peak positions). Although this interpretation was met with much skepticism and never widely

dx.doi.org/10.1021/ar500041m | Acc. Chem. Res. 2014, 47, 2721−2730

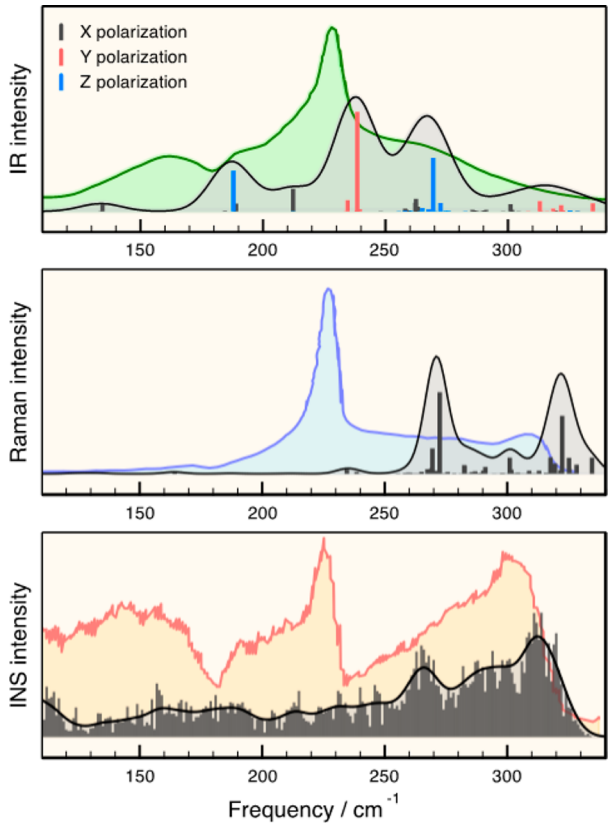

Figure 1. Calculated (gray) and observed IR, Raman, and INS spectra of ice I_h. Reprinted with permission from ref 30, *J. Chem. Phys.* **2012**, *137*, 204505. Copyright 2012 AIP Publishing LLC.

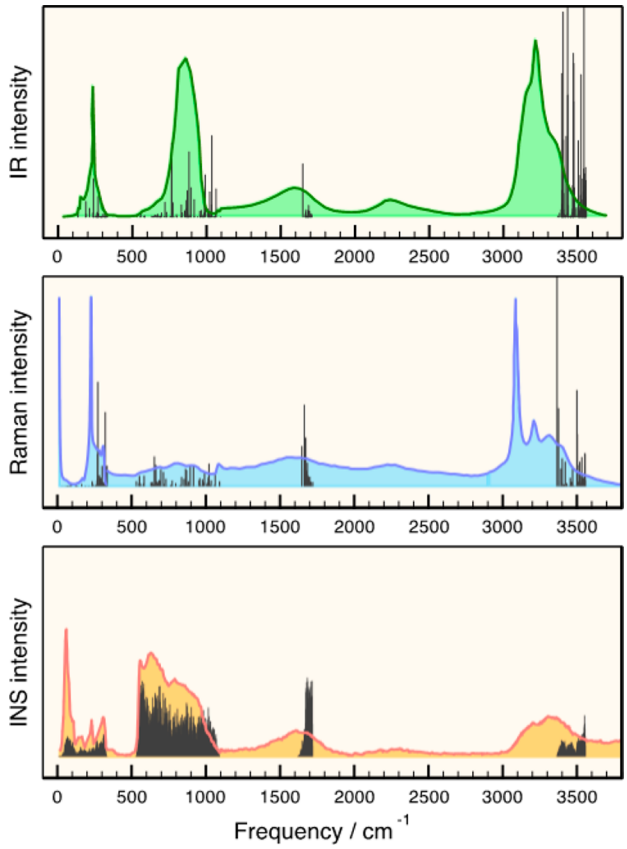

Figure 2. Calculated (gray) and observed IR, Raman, and INS spectra of ice I_h. Reprinted with permission from ref 30, *J. Chem. Phys.* **2012**, *137*, 204505. Copyright 2012 AIP Publishing LLC.

accepted, no alternative explanation was offered until 2012 when our MP2/aug-cc-pVDZ calculation[30] and the plane-wave DFT calculations by Zhang et al.[56] independently resolved this issue.

Our MP2 calculations[30] on the structures and spectra of ice I_h reproduced the two INS peaks in the hydrogen-bond-stretching region (Figure 1) without invoking the assumption about the two types of hydrogen bonds (or any assumption for that matter). They appear in our calculated INS spectrum at about 270 and 310 cm^{-1}. The calculated first peak is somewhat blue-shifted, but this peak is real because the corresponding bands are clearly visible in the calculated IR and Raman spectra. They are, in fact, assignable to the most intense bands in the respective observed spectra in the low-frequency region.

What is the nature of these two INS peaks? Inspection into the normal modes does not reveal much; they both are characterized as hydrogen-bond-stretching vibrations. The transition dipole moments of their IR transitions are more informative. The first (lower-frequency) band has the transition dipole moments along the z (c) axis and the second (higher-frequency) band along the y (b) axis. Furthermore, the latter has much smaller calculated IR intensity, which is corroborated by the experiment. Our conclusion is, therefore, that these two INS peaks are both due to hydrogen-bond-stretching vibrations, but they modulate different Cartesian components of the dipole moment.

The simulated IR, Raman, and INS spectra in the whole frequency range (Figure 2) are also in excellent agreement with the observed. The O−H stretching frequencies (above 3000 cm^{-1}) are overestimated and the combination at about 2200 cm^{-1} is missing in the calculated spectra, both of which are due to the lack of anharmonicity in our potential.

The isotope-concentration dependence of the INS spectra[57] is shown in Figure 3. As more H_2O is replaced by D_2O, some peaks disappear (in 3000−3500 cm^{-1}), some appear (in 2200−2700 cm^{-1}), and others shift their shapes in a complicated way (below 1800 cm^{-1}). All of these are quantitatively explained by our simulation. It is also clear from the figure that HOD exists in abundance owing to rapid H/D exchange, giving rise to the 1500 cm^{-1} peak due to the HOD bending vibration.

The MP2 calculation also reproduces the anomaly of heat capacity[58] (a deviation from the Debye T^3 behavior) of ice I_h at temperatures below 50 K (Figure 4). We have shown that this anomaly arises from the peak in the phonon DOS centered around 60 cm^{-1} and extending to 100 cm^{-1}, which serves as the reservoir of heat at low temperatures.

We have also applied this method at the MP2 and CCSD levels to high-pressure, proton-ordered phase VIII of ice,[33] addressing the pressure dependence of the structure and IR, Raman, and INS spectra in the range of 0−60 GPa to help resolve controversies about possible phase anomalies. Nanda and Beran have performed[48] fragment MP2 and CCSD(T) (CCSD with noniterative triples) calculations of ice XV, establishing its antiferroelectric structure and computationally resolving in 2013 one of the "five unsolved questions" of ice listed by Salzmann et al.[5] in 2011.

Solid Carbon Dioxide

The importance of fully characterizing the properties of carbon dioxide (CO_2) under terrestrially relevant P−T conditions

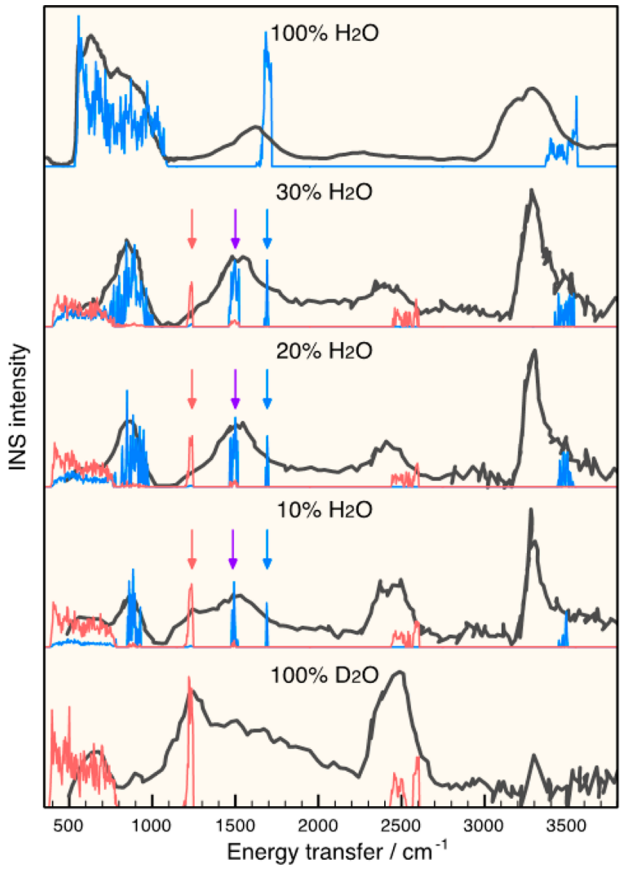

Figure 3. The INS spectra of normal, partially, and fully deuterated ice I_h. The observed spectra in gray; the calculated hydrogen contributions in blue; the calculated deuterium contributions in red. The red, purple, and blue arrows indicate the peaks due to D_2O, HOD, and H_2O bending modes. Reprinted with permission from ref 30, *J. Chem. Phys.* **2012**, *137*, 204505. Copyright 2012 AIP Publishing LLC.

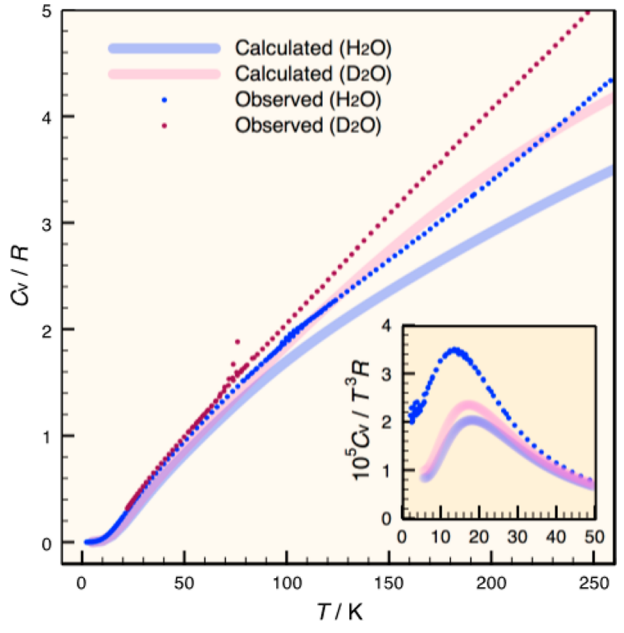

Figure 4. Calculated and observed heat capacities of ice I_h. Reprinted with permission from ref 30, *J. Chem. Phys.* **2012**, *137*, 204505. Copyright 2012 AIP Publishing LLC.

requires no justification.[2,6] CO_2 is also found in asteroids in its ice forms and is, therefore, of astrophysical interest.[6] Nevertheless, our knowledge of the phase diagram of CO_2 is surprisingly limited. The first solid phase, CO_2-III (Figure 5),

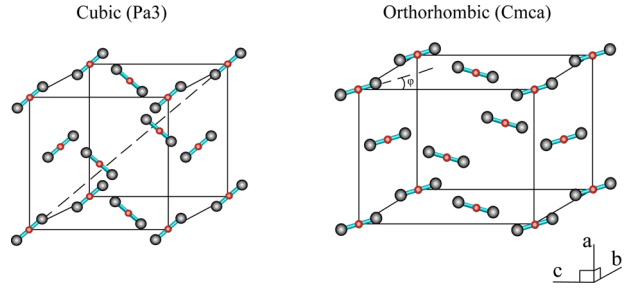

Figure 5. Structure of CO_2-I (*Pa*3) and -III (*Cmca*). Reproduced from ref 32.

other than the familiar cubic phase (CO_2-I or dry ice) was established[59] only in 1994, and many of its properties remain unknown or uncertain. For instance, the reported transition pressures from CO_2-I to -III range from 2.5 to 18 GPa, which is due to large hysteresis of the transition. There is also experimental suggestion that CO_2-III is metastable.

We performed MP2 calculations[32] of the structure, spectra, and phase diagram of CO_2-I and -III under pressure up to 20 GPa and temperature up to 400 K to eliminate some of the uncertainties surrounding the elusive phase III.

Figure 6 shows the calculated equations of state for both phases in comparison with the measured $P-V$ plot. The

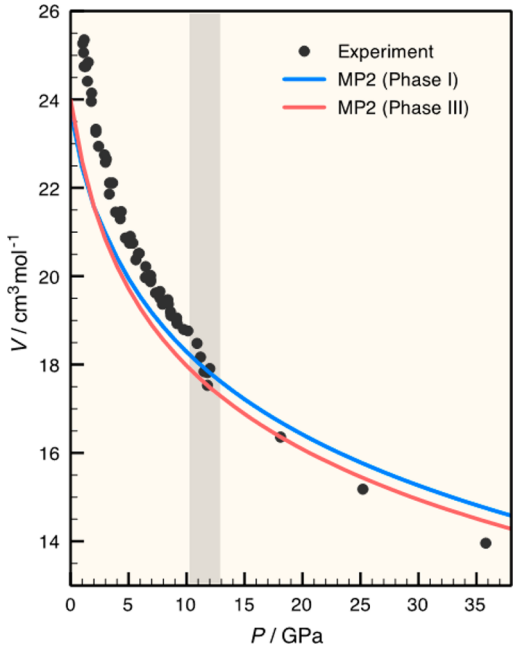

Figure 6. Calculated and observed pressure dependence of volume of CO_2-I and -III. The shaded area is where the transition pressure is suspected to exist. Reproduced from ref 32.

experimental data show a slight, but clearly visible drop in volume at 10−13 GPa, which corresponds to the pressure-induced transition from CO_2-I to -III. Sure enough, our calculated $P-V$ curve for CO_2-III lies lower than that for CO_2-I, which is consistent with this transition. Furthermore, our MP2

dx.doi.org/10.1021/ar500041m | *Acc. Chem. Res.* 2014, 47, 2721−2730

structural parameters of both phases are in agreement with the observed within 0.2 Å and 3°.

We have computed Gibbs energies of CO_2-I and -III and determined their phase boundary, though thermal expansion is neglected. As seen in Figure 7, MP2 places the phase boundary

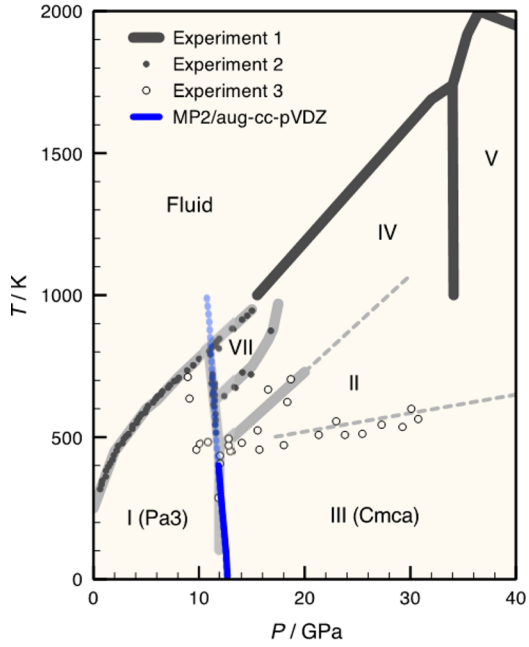

Figure 7. Calculated phase boundary between CO_2-I and -III and experimentally inferred phase diagram. Reproduced from ref 32.

at about 13 GPa at T = 0 K, which is in line with most experimental data. It predicts a small temperature dependence of the transition pressure (reliable only up to 400 K), which is also consistent with various measurements. This is contrasted with a plane-wave DFT study,[60] which was the most reliable theoretical calculation prior to our work and predicted a transition pressure of 16 GPa at T = 0 K and a much greater temperature dependence.

Another compelling piece of evidence of CO_2-III was furnished by vibrational spectroscopy. Hanson[61] reported a dramatic change in the appearance of librational Raman spectra of solid CO_2 between 14.5 and 18.0 GPa, which he assigned to CO_2-I and -III, respectively. No quantitative computational confirmation or assignment of these spectra was made until our study. Figure 8 compares the calculated and observed Raman spectra of CO_2-I and -III under respective comparable pressures. The agreement confirms the correctness of the original interpretation of Hanson. This was the first time that the structural and spectral information on CO_2-III were mutually verified through quantitative calculations.

There is another fascinating story about the high-pressure chemistry of CO_2.[31]

The symmetric stretching vibration (ω_1) and the first overtone of bending vibration ($2\omega_2$) in the CO_2 molecule is well-known to undergo strong anharmonic mode−mode coupling known as Fermi resonance.[62,63] As a result, there are two intense bands (ν_+ and ν_-) in the salient region of its Raman spectra, instead of just one band from ω_1. The two bands are both linear combinations of optically bright ω_1 and dark $2\omega_2$, which are separated by about 100 cm^{-1}. This

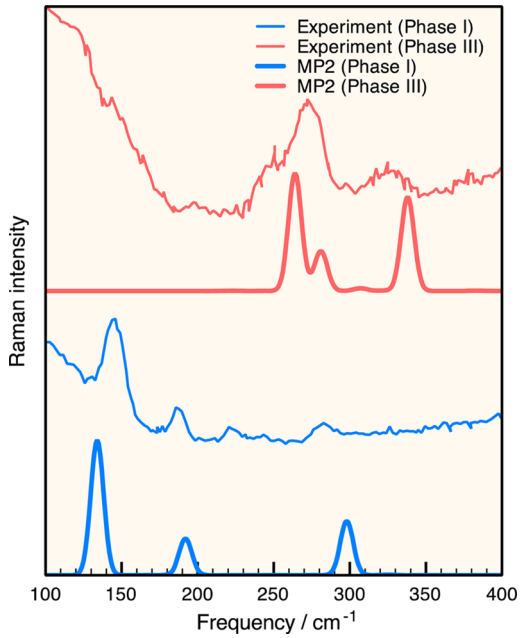

Figure 8. Calculated and observed Raman spectra of CO_2-I (at 14.5 GPa) and -III (at 18.0 GPa). Reproduced from ref 32.

resonance occurs in all of the gas, liquid, and solid phases of CO_2.

What makes the *condensed-phase* Fermi resonance particularly interesting is the fact that it can be pressure-tuned and even nearly turned off. Pressure can alter the harmonic frequencies of ω_1 and $2\omega_2$ differently, which are then brought to off resonance. Geochemists have utilized this property of CO_2 and developed an accurate *geobarometer* for minerals with CO_2 inclusions;[64−66] by measuring the Fermi dyad frequency difference or intensity ratio, geochemists can determine the residual pressure experienced by CO_2 trapped in minerals. This pressure, in turn, carries a critical piece of information about the depth at which the minerals were entrained and thus about the mantle tectonics. In other words, a tiny bubble of CO_2 trapped in a rock remembers the formation history of the rock across eons.

Quantitative computational explanation of this phenomenon is challenging. The calculation must be accurate enough to account for the delicate balance of the resonating harmonic states' positions (ω_1 and $2\omega_2$) and the anharmonic coupling between them as well as their pressure dependence. To achieve this, we took a hybrid approach:[31] we used an accurate quartic force field (QFF) of an *isolated* CO_2 molecule obtained by the CCSD(T) method,[63] whereas we obtained the pressure dependence of the quadratic force constants from the embedded-fragment MP2 calculation of solid CO_2-I under up to 10 GPa of pressure. Although MP2 is not accurate enough for the absolute values of the frequencies, it is quantitative for pressure dependence (see Figure 9). Note that the bending modes (between 600 and 700 cm^{-1}) decrease in frequency with pressure, while all the other modes increase, which is the primary cause of pressure tuning of the Fermi resonance. Combining these two pieces of information, we could reproduce the observed pressure dependence of the Fermi dyad frequencies and intensity ratios quantitatively, as shown in Figure 10.

dx.doi.org/10.1021/ar500041m | Acc. Chem. Res. 2014, 47, 2721−2730

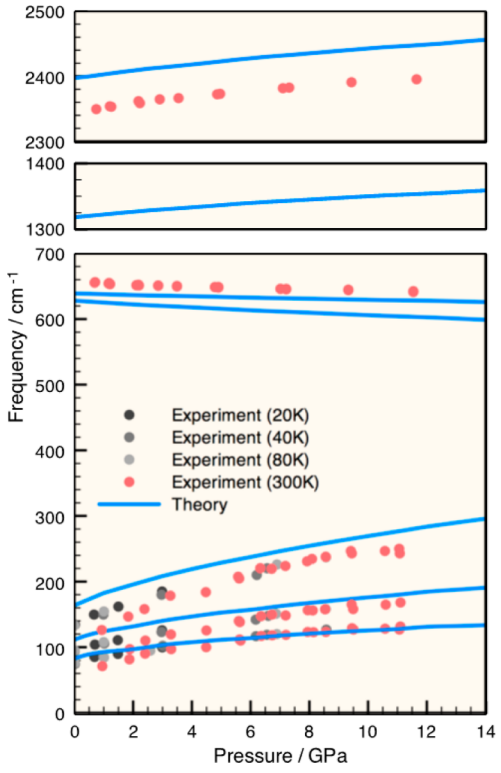

Figure 9. Pressure dependence of the IR and Raman band positions of CO_2-I. Reprinted with permission from ref 31, *J. Chem. Phys.* **2013**, *138*, 074501. Copyright 2013 AIP Publishing LLC.

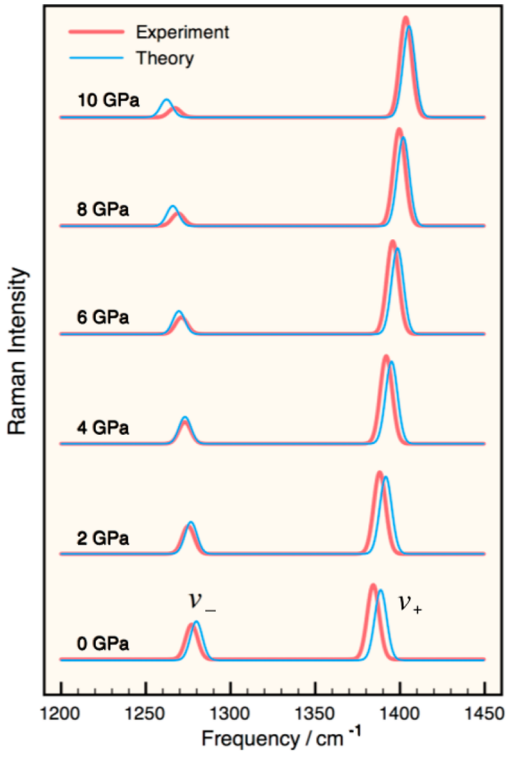

Figure 10. Calculated and observed Raman spectra of CO_2-I in the symmetric stretching (Fermi-resonance) region. Reprinted with permission from ref 31, *J. Chem. Phys.* **2013**, *138*, 074501. Copyright 2013 AIP Publishing LLC.

Solid Formic Acid

Solid formic acid is a hydrogen-bonded crystal that is strongly anisotropic and is, therefore, treatable as a one-dimensional solid. There are at least three possible polymorphs in one dimension: the α and β_1 structures that consist of *syn*-HCOOH and the β_2 structure made from *anti*-HCOOH (Figure 11). As an isolated molecule, the *syn* isomer is more stable than the *anti* isomer by 16.3 kJ mol^{-1}.

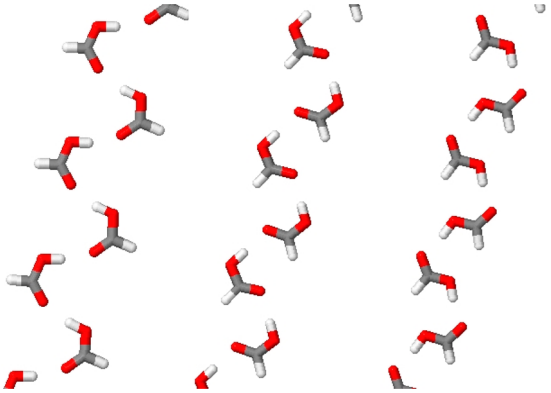

Figure 11. The α (left), β_1 (middle), and β_2 (right) forms of solid formic acid.

There has been a controversy as to which of these three structures is correct in the solid state. The IR spectra of the crystal with various isotope substitutions were reported by Millikan and Pitzer[67] and analyzed by Miyazawa and Pitzer[68] in terms of the β_1 structure proposed by an earlier X-ray diffraction study. Many intense bands were found to be doublets, which they assigned to pairs of in-phase and out-of-phase vibrations (both IR active) of adjacent molecules.

Mikawa et al.[69] disagreed with this interpretation, suggesting that the doublets were due to coexistence of two structures, specifically, α and β_1. A subsequent neutron diffraction study[70] sided with Miyazawa and Pitzer,[68] establishing the β_1 form of the crystal at 4.5 K. However, Zelsmann et al.[71] observed a phase transition occurring between 207 and 218 K above which the β_1 and β_2 structures were speculated to coexist. Wiechert et al.[72] also detected a pressure-induced phase transition at 4.5 GPa, which they viewed as simultaneous proton transfer and resulting β_1 to β_2 tautomerization.

Our BSSE-corrected MP2/aug-cc-pVTZ and CCSD/aug-cc-pVDZ calculations[26] on energies and MP2/aug-cc-pVDZ calculations[26] on structures and spectra clearly support the original interpretation of Miyazawa and Pitzer,[68] although they do not rule out possible phase transitions and polymorphism.

All of our calculations are in agreement on the stability order of $\beta_1 > \beta_2 > \alpha$. This along with the fact that the calculated lattice constant of the α form is far from the observed value (while those of β_1 and β_2 are consistent with the observed), we can rule out the α form and, therefore, the interpretation of Mikawa et al.,[69] which involves the α and β_1 polymorphism.

The observed IR and Raman bands are readily assignable to the MP2-calculated normal modes of the β_1 form, and each band doublet can be explained by the proximity of the frequencies of the in-phase and out-of-phase vibrations of one phonon branch (Figure 12) in accordance with Miyazawa and Pitzer.[68]

dx.doi.org/10.1021/ar500041m | *Acc. Chem. Res.* 2014, 47, 2721−2730

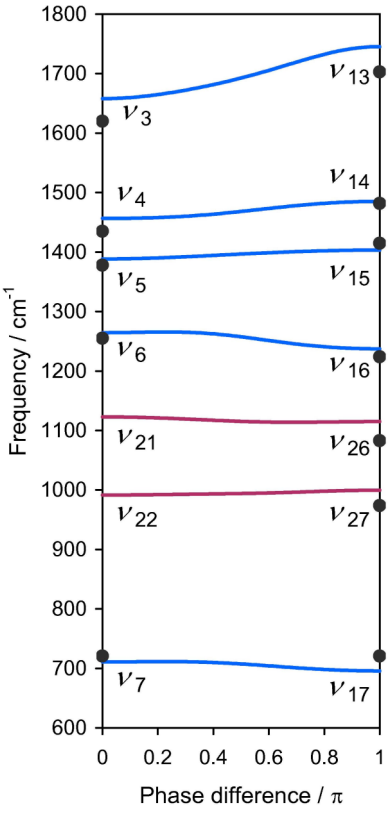

Figure 12. Calculated phonon dispersions (blue) in the β_1 form and observed IR and Raman band positions (red) of solid formic acid. Reprinted with permission from ref 26, *J. Chem. Phys.* **2008**, *129*, 204104. Copyright 2008 AIP Publishing LLC.

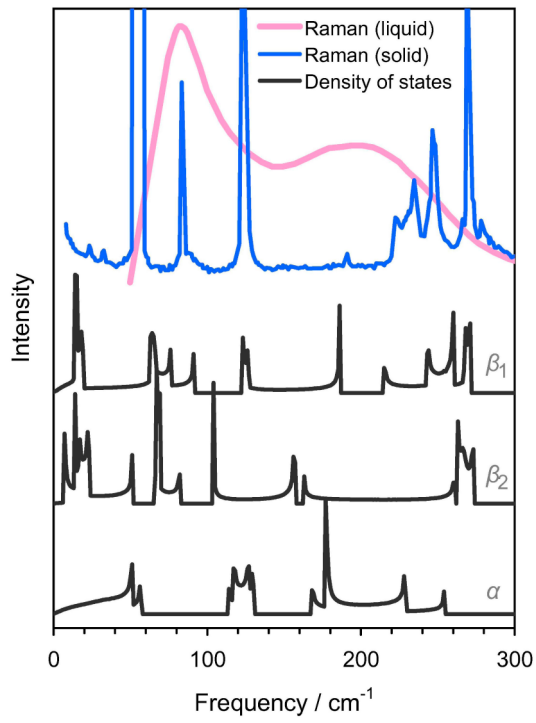

Figure 13. Calculated phonon DOS (black) of the β_1 (top), β_2 (middle), and α (bottom) forms and the observed Raman spectra of solid (blue) and liquid (red) formic acid. Reprinted with permission from ref 26, *J. Chem. Phys.* **2008**, *129*, 204104. Copyright 2008 AIP Publishing LLC.

Furthermore, the observed Raman spectrum in the low-frequency region most closely resembles the phonon DOS of the β_1 form (Figure 13). In fact, the sample used in this measurement cannot contain the β_2 or α form because no peak in the observed spectrum seems to be uniquely assignable to the calculated peaks of the β_2 or α form.

Finally, Figure 14 attests to the good agreement between the MP2-simulated INS spectra of the β_1 form and the observed spectra for three isotopomers. While not shown in this figure, the simulated spectra of the β_2 form disagree with the observed spectra in the low-energy region, and those of the α form disagree everywhere below 1000 cm^{-1}. This further reinforces the foregoing conclusion: the samples used in these spectroscopic measurements consist of the pristine β_1 form.

CONCLUSION

The success of the linear combination of atomic orbital molecular orbital (LCAO-MO) theory for molecular electronic structures derives from the fact that the Coulomb forces exerted by nuclei are so strong that a majority of electrons in a molecule experience nearly atomic environments. We can then expect that electrons in molecular clusters, crystals, and liquids are largely in molecular environments and may accurately be describable by linear combination of *molecular* orbital *crystal* orbital (LCMO-CO) theory, which is what the embedded-fragment scheme implements. The unparalleled advantage of this scheme is that we can immediately inherit the whole arsenal of molecular electronic structure theories and software developed and refined in the last half century and reconstruct the crystal properties from those of the constituent molecules

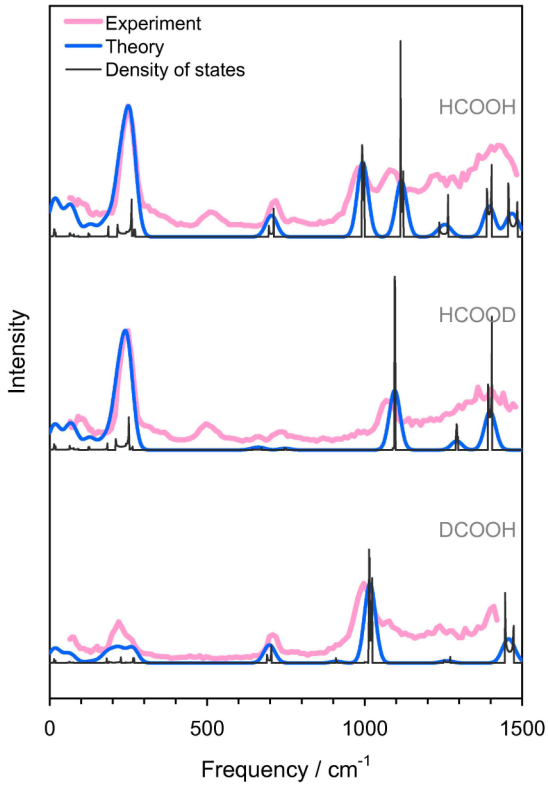

Figure 14. Simulated (blue) and observed (red) INS spectra of the β_1 form of solid HCOOH, HCOOD, and DCOOH. Reprinted with permission from ref 26, *J. Chem. Phys.* **2008**, *129*, 204104. Copyright 2008 AIP Publishing LLC.

dx.doi.org/10.1021/ar500041m | *Acc. Chem. Res.* 2014, 47, 2721−2730

obtained at the MP2, CCSD, or higher level. The applications described in this Account underscore the enormous breadth of crystal properties we can already address quantitatively and relatively easily to draw important conclusions about nature's most important crystals such as ice and dry ice. It is already possible to treat nonperiodic molecular crystals, and it should in principle be applicable to molecular liquids, ultimately leading to ab initio phase diagrams. It is also not unthinkable that this scheme be extended to ionic crystals, covalent crystals, and even metals and superconductors in the future.

AUTHOR INFORMATION

Corresponding Author

*E-mail: sohirata@illinois.edu.

Present Addresses

†State Key Laboratory of Precision Spectroscopy, Department of Physics, Institute of Theoretical and Computational Science, East China Normal University.

‡Department of Chemistry, University of Chicago.

Funding

We thank the U.S. National Science Foundation (Grant CHE-1118616), the U.S. Department of Energy (Grants DE-FG02-11ER16211 and SciDAC DE-FG02-12ER46875), the Camille & Henry Dreyfus Foundation, the Research Corporation for Science Advancement, and the Japan Science and Technology Agency (CREST).

Notes

The authors declare no competing financial interest.

Biographies

So Hirata received B.S. (1994) and M.S. (1996) from University of Tokyo and Ph.D. (1998) from Graduate University for Advanced Studies all in chemistry. Following postdoctoral studies at University of California, Berkeley, and University of Florida, he became a Senior Research Scientist (2001−2004) at Pacific Northwest National Laboratory. He had been on the faculty of University of Florida in 2004−2010 before he became an Alumni Research Scholar Professor of Chemistry (2010) and a Blue Waters Professor (2014) at University of Illinois at Urbana−Champaign.

Kandis Gilliard received a B.S. in chemistry (2007) from Temple University. She had been a forensic scientist at the Philadelphia Police Department before she began pursuing a Ph.D. in chemistry at University of Illinois at Urbana−Champaign. She was a winner of the 2013 Spring American Chemical Society Women Chemists Committee Eli Lilly Travel Grant Award.

Xiao He received a B.S. in physics (2003), M.S. in chemistry (2006) from Nanjing University, and Ph.D. in chemistry (2010) from University of Florida under the supervision of Professor Kenneth Merz. He was trained as a postdoctoral researcher at University of Illinois at Urbana−Champaign (2011−2012), where his advisor was Professor So Hirata. He is currently an Associate Professor of State Key Laboratory of Precision Spectroscopy at East China Normal University.

Jinjin Li received a B.S. in applied physics (2007) from Tianjin University of Technology and Ph.D. in physics (2012) from Shanghai Jiao Tong University, where she was a Lin-Yang Scholar. She is currently a postdoctoral researcher at University of Illinois at Urbana−Champaign.

Olaseni Sode received a B.S. in chemistry and B.A. in French (2006) from Morehouse College and Ph.D. in chemistry (2012) from University of Illinois at Urbana−Champaign, where he was a Roger Adams fellow and a GAANN fellow. Currently, he is a postdoctoral scholar at University of Chicago.

REFERENCES

(1) Hemley, R. J. The Element of Uncertainty. *Nature* **2000**, *404*, 240−241.
(2) Hemley, R. J. Effects of High Pressure on Molecules. *Annu. Rev. Phys. Chem.* **2000**, *51*, 763−800.
(3) Fletcher, N. H. *The Chemical Physics of Ice*; Cambridge University Press: New York, 1970.
(4) Petrenko, V. F.; Whitworth, R. W. *Physics of Ice*; Oxford University Press: New York, 1999.
(5) Salzmann, C. G.; Radaelli, P. G.; Slater, B.; Finney, J. L. The Polymorphism of Ice: Five Unresolved Questions. *Phys. Chem. Chem. Phys.* **2011**, *13*, 18468−18480.
(6) Santoro, M.; Gorelli, F. A. High Pressure Solid State Chemistry of Carbon Dioxide. *Chem. Soc. Rev.* **2006**, *35*, 918−931.
(7) McMahon, J. M.; Morales, M. A.; Pierleoni, C.; Ceperley, D. M. The Properties of Hydrogen and Helium under Extreme Conditions. *Rev. Mod. Phys.* **2012**, *84*, 1607−1653.
(8) Lieserowitz, L.; Stoddart, J. F. Molecular Crystals. *Curr. Opin. Solid State Mater. Sci.* **1998**, *3*, 397−398.
(9) Inokuma, Y.; Kawano, M.; Fujita, M. Crystalline Molecular Flasks. *Nat. Chem.* **2011**, *3*, 349−358.
(10) Zhou, H. C.; Long, J. R.; Yaghi, O. M. Introduction to Metal−Organic Frameworks. *Chem. Rev.* **2012**, *112*, 673−674.
(11) Dlott, D. D. Ultrafast Spectroscopy of Shock Waves in Molecular Materials. *Annu. Rev. Phys. Chem.* **1999**, *50*, 251−278.
(12) Wen, S. H.; Beran, G. J. O. Accidental Degeneracy in Crystalline Aspirin: New Insights from High-Level Ab Initio Calculations. *Cryst. Growth Des.* **2012**, *12*, 2169−2172.
(13) Bernstein, J. *Polymorphism in Molecular Crystals*; Clarendon Press: Oxford, 2002.
(14) McCrone, W. C. Polymorphism. In *Physics and Chemistry of the Organic Solid State*; Fox, D., Labes, M. M., Weissberger, A., Eds.; Wiley: New York, 1965; Vol. 2; pp 725−767.
(15) Suhai, S. Quasiparticle Energy-Band Structures in Semiconducting Polymers: Correlation-Effects on the Band-Gap in Polyacetylene. *Phys. Rev. B* **1983**, *27*, 3506−3518.
(16) Stoll, H. Correlation Energy of Diamond. *Phys. Rev. B* **1992**, *46*, 6700−6704.
(17) Hirata, S.; Podeszwa, R.; Tobita, M.; Bartlett, R. J. Coupled-Cluster Singles and Doubles for Extended Systems. *J. Chem. Phys.* **2004**, *120*, 2581−2592.
(18) Pisani, C.; Busso, M.; Capecchi, G.; Casassa, S.; Dovesi, R.; Maschio, L.; Zicovich-Wilson, C.; Schütz, M. Local MP2 Electron Correlation Method for Nonconducting Crystals. *J. Chem. Phys.* **2005**, *122*, No. 094113.
(19) Shepherd, J. J.; Grüneis, A.; Booth, G. H.; Kresse, G.; Alavi, A. Convergence of Many-Body Wave-Function Expansions Using a Plane-Wave Basis: From Homogeneous Electron Gas to Solid State Systems. *Phys. Rev. B* **2012**, *86*, No. 035111.
(20) Nanda, K. D.; Beran, G. J. O. Prediction of Organic Molecular Crystal Geometries from MP2-Level Fragment Quantum Mechanical/Molecular Mechanical Calculations. *J. Chem. Phys.* **2012**, *137*, No. 174106.
(21) Grimme, S. Accurate Description of van der Waals Complexes by Density Functional Theory Including Empirical Corrections. *J. Comput. Chem.* **2004**, *25*, 1463−1473.
(22) Hirata, S.; Yagi, K. Predictive Electronic and Vibrational Many-Body Methods for Molecules and Macromolecules. *Chem. Phys. Lett.* **2008**, *464*, 123−134.
(23) Shavitt, I.; Bartlett, R. J. *Many-Body Methods in Chemistry and Physics*; Cambridge University Press: Cambridge, U.K., 2009.
(24) Hirata, S.; Valiev, M.; Dupuis, M.; Xantheas, S. S.; Sugiki, S.; Sekino, H. Fast Electron Correlation Methods for Molecular Clusters in the Ground and Excited States. *Mol. Phys.* **2005**, *103*, 2255−2265.

(25) Kamiya, M.; Hirata, S.; Valiev, M. Fast Electron Correlation Methods for Molecular Clusters without Basis Set Superposition Errors. *J. Chem. Phys.* **2008**, *128*, No. 074103.
(26) Hirata, S. Fast Electron-Correlation Methods for Molecular Crystals: An Application to the α, β_1, and β_2 Polymorphs of Solid Formic Acid. *J. Chem. Phys.* **2008**, *129*, No. 204104.
(27) Sode, O.; Keçeli, M.; Hirata, S.; Yagi, K. Coupled-Cluster and Many-Body Perturbation Study of Energies, Structures, and Phonon Dispersions of Solid Hydrogen Fluoride. *Int. J. Quantum Chem.* **2009**, *109*, 1928−1939.
(28) Sode, O.; Hirata, S. Second-Order Many-Body Perturbation Study of Solid Hydrogen Fluoride. *J. Phys. Chem. A* **2010**, *114*, 8873−8877.
(29) Sode, O.; Hirata, S. Second-Order Many-Body Perturbation Study of Solid Hydrogen Fluoride under Pressure. *Phys. Chem. Chem. Phys.* **2012**, *14*, 7765−7779.
(30) He, X.; Sode, O.; Xantheas, S. S.; Hirata, S. Second-Order Many-Body Perturbation Study of Ice Ih. *J. Chem. Phys.* **2012**, *137*, No. 204505.
(31) Sode, O.; Keçeli, M.; Yagi, K.; Hirata, S. Fermi Resonance in Solid CO_2 under Pressure. *J. Chem. Phys.* **2013**, *138*, No. 074501.
(32) Li, J.; Sode, O.; Voth, G. A.; Hirata, S. A Solid-Solid Phase Transition in Carbon Dioxide at High Pressure and Intermediate Temperatures. *Nat. Commun.* **2013**, *4*, No. 2647.
(33) Gilliard, K.; Sode, O.; Hirata, S. Second-Order Many-Body Perturbation and Coupled-Cluster Singles and Doubles Study of Ice VIII. *J. Chem. Phys.* **2014**, in press.
(34) Gordon, M. S.; Fedorov, D. G.; Pruitt, S. R.; Slipchenko, L. V. Fragmentation Methods: A Route to Accurate Calculations on Large Systems. *Chem. Rev.* **2012**, *112*, 632−672.
(35) Beran, G. J. O.; Hirata, S. Fragment and Localized Orbital Methods in Electronic Structure Theory. *Phys. Chem. Chem. Phys.* **2012**, *14*, 7559−7561.
(36) Fedorov, D. G.; Kitaura, K. Extending the Power of Quantum Chemistry to Large Systems with the Fragment Molecular Orbital Method. *J. Phys. Chem. A* **2007**, *111*, 6904−6914.
(37) Hirata, S. Quantum Chemistry of Macromolecules and Solids. *Phys. Chem. Chem. Phys.* **2009**, *11*, 8397−8412.
(38) Manby, F. *Accurate Condensed-Phase Quantum Chemistry*; CRC Press: Boca Raton, FL, 2010.
(39) Richard, R. M.; Herbert, J. M. A Generalized Many-Body Expansion and a Unified View of Fragment-Based Methods in Electronic Structure Theory. *J. Chem. Phys.* **2012**, *137*, No. 064113.
(40) Stoll, H.; Paulus, B.; Fulde, P. On the Accuracy of Correlation-Energy Expansions in Terms of Local Increments. *J. Chem. Phys.* **2005**, *123*, No. 144108.
(41) Manby, F. R.; Alfè, D.; Gillan, M. J. Extension of Molecular Electronic Structure Methods to the Solid State: Computation of the Cohesive Energy of Lithium Hydride. *Phys. Chem. Chem. Phys.* **2006**, *8*, 5178−5180.
(42) Podeszwa, R.; Rice, B. M.; Szalewicz, K. Predicting Structure of Molecular Crystals from First Principles. *Phys. Rev. Lett.* **2008**, *101*, No. 115503.
(43) Ringer, A. L.; Sherrill, C. D. First Principles Computation of Lattice Energies of Organic Solids: The Benzene Crystal. *Chem.—Eur. J.* **2008**, *14*, 2542−2547.
(44) Podeszwa, R.; Rice, B. M.; Szalewicz, K. Crystal Structure Prediction for Cyclotrimethylene Trinitramine (RDX) from First Principles. *Phys. Chem. Chem. Phys.* **2009**, *11*, 5512−5518.
(45) Schwerdtfeger, P.; Assadollahzadeh, B.; Hermann, A. Convergence of the Møller-Plesset Perturbation Series for the fcc Lattices of Neon and Argon. *Phys. Rev. B* **2010**, *82*, No. 205111.
(46) Beran, G. J. O.; Nanda, K. Predicting Organic Crystal Lattice Energies with Chemical Accuracy. *J. Phys. Chem. Lett.* **2010**, *1*, 3480−3487.
(47) Collins, M. A. Ab Initio Lattice Dynamics of Nonconducting Crystals by Systematic Fragmentation. *J. Chem. Phys.* **2011**, *134*, No. 164110.
(48) Nanda, K.; Beran, G. What Governs the Proton Ordering in Ice XV? *J. Phys. Chem. Lett.* **2013**, *4*, 3165−3169.
(49) Kitaura, K.; Sawai, T.; Asada, T.; Nakano, T.; Uebayasi, M. Pair Interaction Molecular Orbital Method: An Approximate Computational Method for Molecular Interactions. *Chem. Phys. Lett.* **1999**, *312*, 319−324.
(50) Blount, E. I. Formalisms of Band Theory. *Solid State Phys.* **1962**, *13*, 305−373.
(51) Resta, R. Macroscopic Polarization in Crystalline Dielectrics: The Geometric Phase Approach. *Rev. Mod. Phys.* **1994**, *66*, 899−915.
(52) Stoll, H. On the Correlation-Energy of Graphite. *J. Chem. Phys.* **1992**, *97*, 8449−8454.
(53) Stoll, H.; Paulus, B.; Fulde, P. An Incremental Coupled-Cluster Approach to Metallic Lithium. *Chem. Phys. Lett.* **2009**, *469*, 90−93.
(54) Gräfenstein, J.; Stoll, H.; Fulde, P. Computation of the Valence-Band of Diamond by Means of Local Increments. *Chem. Phys. Lett.* **1993**, *215*, 611−616.
(55) Li, J. C.; Ross, D. K. Evidence for Two Kinds of Hydrogen-Bond in Ice. *Nature* **1993**, *365*, 327−329.
(56) Zhang, P.; Tian, L.; Zhang, Z. P.; Shao, G.; Li, J. C. Investigation of the Hydrogen Bonding in Ice Ih by First-Principles Density Function Methods. *J. Chem. Phys.* **2012**, *137*, No. 044504.
(57) Li, J. C. Inelastic Neutron Scattering Studies of Hydrogen Bonding in Ices. *J. Chem. Phys.* **1996**, *105*, 6733−6755.
(58) Flubacher, P.; Leadbetter, A. J.; Morrison, J. A. Heat Capacity of Ice at Low Temperatures. *J. Chem. Phys.* **1960**, *33*, 1751−1755.
(59) Aoki, K.; Yamawaki, H.; Sakashita, M.; Gotoh, Y.; Takemura, K. Crystal-Structure of the High-Pressure Phase of Solid CO_2. *Science* **1994**, *263*, 356−358.
(60) Bonev, S. A.; Gygi, F.; Ogitsu, T.; Galli, G. High-Pressure Molecular Phases of Solid Carbon Dioxide. *Phys. Rev. Lett.* **2003**, *91*, No. 065501.
(61) Hanson, R. C. A New High-Pressure Phase of Solid CO_2. *J. Phys. Chem.* **1985**, *89*, 4499−4501.
(62) Wilson Jr., E. B.; Decius, J. C.; Cross, P. C. *Molecular Vibrations*; Dover: New York, 1955.
(63) Rodriguez-Garcia, V.; Hirata, S.; Yagi, K.; Hirao, K.; Taketsugu, T.; Schweigert, I.; Tasumi, M. CO_2 Fermi Resonance: An Accurate Prediction by Electronic Coupled-Cluster and Vibrational Configuration-Interaction Methods. *J. Chem. Phys.* **2007**, *126*, No. 124303.
(64) Roedder, E. Geobarometry of Ultramafic Xenoliths from Loihi Seamount, Hawaii, on the Basis of CO_2 Inclusions in Olivine. *Earth Planet. Sci. Lett.* **1983**, *66*, 369−379.
(65) Navon, O. High Internal-Pressures in Diamond Fluid Inclusions Determined by Infrared-Absorption. *Nature* **1991**, *353*, 746−748.
(66) Schrauder, M.; Navon, O. Solid Carbon Dioxide in a Natural Diamond. *Nature* **1993**, *365*, 42−44.
(67) Millikan, R. C.; Pitzer, K. S. The Infrared Spectra of Dimeric and Crystalline Formic Acid. *J. Am. Chem. Soc.* **1958**, *80*, 3515−3521.
(68) Miyazawa, T.; Pitzer, K. S. Internal Rotation and Infrared Spectra of Formic Acid Monomer and Normal Coordinate Treatment of Out-of-Plane Vibrations of Monomer, Dimer, and Polymer. *J. Chem. Phys.* **1959**, *30*, 1076−1086.
(69) Mikawa, Y.; Jakobsen, R. J.; Brasch, J. W. Infrared Evidence of Polymorphism in Formic Acid Crystals. *J. Chem. Phys.* **1966**, *45*, 4750−4751.
(70) Albinati, A.; Rouse, K. D.; Thomas, M. W. Neutron Powder Diffraction Analysis of Hydrogen-Bonded Solids. II. Structural Study of Formic-Acid at 4.5 K. *Acta Crystallogr.* **1978**, *B34*, 2188−2190.
(71) Zelsmann, H. R.; Bellon, F.; Marechal, Y.; Bullemer, B. Polymorphism in Crystalline Formic Acid. *Chem. Phys. Lett.* **1970**, *6*, 513−515.
(72) Wiechert, D.; Mootz, D.; Dahlems, T. The Formic Acid 1D Array with H Bonds All Reversed: Structure of a Co-Crystal with Hydrogen Fluoride. *J. Am. Chem. Soc.* **1997**, *119*, 12665−12666.